JTTEE5 17:551–563
DOI: 10.1007/s11666-008-9206-0
1059-9630/$19.00 © ASM International

Optical Diagnostics Study of Gas Particle Transport Phenomena in Cold Gas Dynamic Spraying and Comparison with Model Predictions

Sudharshan Phani Pardhasaradhi, Vishnukanthan Venkatachalapathy, Shrikant V Joshi, and Sundararajan Govindan

(Submitted January 20, 2008; in revised form July 3, 2008)

Cold gas dynamic spraying (CGDS), a relatively new thermal spraying technique has drawn a lot of attention due to its inherent capability to deposit a wide range of materials at relatively low-operating temperatures. A De Laval nozzle, used to accelerate the powder particles, is the key component of the coating equipment. Knowledge concerning the nozzle design and effect of process parameters is essential to understand the coating process and to enable selection of appropriate parameters for enhanced coating properties. The present work employs a one-dimensional isentropic gas flow model in conjunction with a particle acceleration model to calculate particle velocities. A laser illumination-based optical diagnostic system is used for validation studies to determine the particle velocity at the nozzle exit for a wide range of process and feedstock parameters such as stagnation temperature, stagnation pressure, powder feed rate, particle size and density. The relative influence of process and feedstock parameters on particle velocity is presented in this work.

Keywords cold spray, modeling of cold spray, nozzle design, powder particle diagnostics, process parameters

1. Introduction

Cold Gas Dynamic Spraying (CGDS) process is a relatively new thermal spraying process in which powder particles (typically 1-50 μm in diameter) are accelerated to velocities of the order of 500-1000 m/s in a supersonic jet of high-pressure gas (Ref 1). Upon striking a target surface, the powder particles undergo severe plastic deformation and form a coating on the target, which is built up layer by layer. The process details have been elaborated elsewhere (Ref 2).

A De Laval nozzle, used to accelerate the powder particles, is the key component of the coating equipment. Knowledge concerning the nozzle design and effect of process parameters is essential to understand the coating process and to enable selection of appropriate parameters for enhanced coating properties. Particle velocity is known to be one of the most important parameter effecting the coating properties. Dykhuzien et al. (Ref 3) used an isentropic gas flow model and a particle acceleration model with a few assumptions to derive a closed form equation for the particle velocity. Alkhimov et al. (Ref 4) derived an empirical equation for particle velocity based on the experimental data. Jodoin (Ref 5) used a two-dimensional flow model to study the effect of exit Mach number on particle velocity upon impact. Stoltenhoff et al. (Ref 6) employed computational fluid dynamics (CFD) to calculate the particle velocity for different gas inlet conditions for the case of copper powder. Grujicic et al. (Ref 7) employed a one-dimensional model to predict the particle velocity at nozzle exit and particle behavior upon impact with a substrate during CGDS. Li et al. (Ref 8) carried out simulations using FLUENT to study the effect of throat & exit area and diverging section length on the particle flow and to optimize the nozzle design for different inlet conditions. A comparative study of the difference in particle flow for a converging barrel (CB) and converging diverging (CD) nozzle used in cold spray was reported by Li et al. (Ref 9). Jen et al. (Ref 10) reported the effect of friction on the gas dynamic flow through the CD nozzle. The effect of particle size on the acceleration of the particles was also reported by Jen et al. (Ref 10). The effect of particle size range and inlet gas pressure during deposition of Titanium coatings by CGDS, along with modeling results from a one-dimensional model, was reported by Marrocco et al. (Ref 11). Taylor et al. (Ref 12) reported the effect of particle loading on the particle velocity and the coating properties of copper coatings. Jodoin et al. (Ref 13) used a high-speed CCD camera-based system to measure the velocity

Sudharshan Phani Pardhasaradhi, Vishnukanthan Venkatachalapathy, Shrikant V Joshi, and **Sundararajan Govindan**, International Advanced Research Centre for Powder Metallurgy and New Materials (ARCI), Balapur (P.O.), Hyderabad 500 005, India. Contact e-mail: spphani@yahoo.com.

of nickel powder particles for different stagnation temperatures in nitrogen and helium. Jingwei Wu et al. (Ref 14) employed a similar technique to measure the velocities for Al-Si particles sprayed using a nozzle with circular exit. Fukanuma et al. (Ref 15) used a different system (DPV-2000) to measure the particle velocity for different inlet conditions for SS316 powder. Ning et al. (Ref 16) studied the effect of powder morphology and gas pre heat temperature on particle velocity using the SprayWatch optical diagnostics system. Karimi et al. (Ref 17) employed CFD to model the flow through a oval shaped nozzle and compared the model predictions with the velocity measured by a Laser Doppler anemometer (LDA). Li et al. (Ref 18) used a diagnostics system developed at Xi'an Jiaotong university to measure the particle velocity for copper particles of various sizes and compared the results with those of a two-dimensional axisymmetric model.

The above literature survey thus indicates that several prior studies have attempted to propose mathematical models or employed CFD tools (Ref 3-12) to model the particle flow through the De Laval nozzle and recently some studies on the use of optical diagnostics techniques for particle velocity measurement have also been attempted (Ref 13-18). However, a comprehensive study involving measurement of particle velocity for a wide range of powders of different sizes and densities at different gas inlet conditions has not been attempted. Also, most of the prior studies using optical diagnostic techniques have been carried out for nozzles with circular exit. Hence, the present study focuses on determining the particle velocity at the exit of the De Laval nozzle with rectangular exit over a wide range of stagnation pressure, stagnation temperature and powder feed rate for powders of different densities and sizes. The study also employs isentropic gas flow and particle acceleration models to numerically determine the particle velocities. This would enable a comprehensive understanding of the effect of process parameters and feedstock conditions on the particle velocity resulting in the formulation of a process map, which could be of immense help in parameter selection.

2. Experimental Procedure

2.1 Parameter Selection and Design of Experiments

Powders were sprayed using the in house facility for cold spraying. A De Laval nozzle with a rectangular exit was used for the present study. The throat and exit dimensions were 3 × 3 mm and 10 × 3 mm, respectively, with a straight diverging section. The nozzle had an exit to throat area ratio of 3.33 and a diverging section length (X_o) of 102 mm. The powder particles were injected at the inlet of the converging section. Compressed air was used as the process gas as well as the powder carrier gas. Velocity measurements were made at the exit of the nozzle up to a distance of 6 mm within which no significant

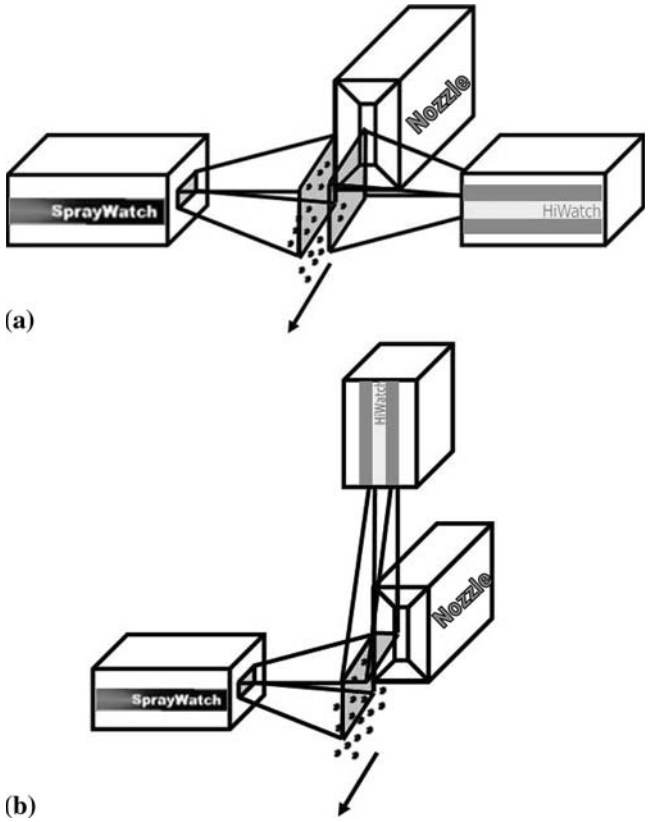

Fig. 1 Different experimental setups of high-speed imaging system (a) background illumination and (b) sheet laser illumination

change in velocity with the spray distance was observed. Thus, the measuring volume during the course of this study was 10 × 3 × 6 mm^3.

Modeling studies have indicated the stagnation temperature and stagnation pressure to be important parameters in determining the particle velocity at the exit of the nozzle. Also, earlier studies have indicated powder feed rate to have some effect on coating properties (Ref 12, 19). Hence, stagnation temperature, stagnation pressure and powder feed rate were chosen to be the major process variables. Also, modeling studies indicate the strong influence of powder size and density on the particle velocity. Hence, particle size and density were chosen to be the feedstock variables. An experimental matrix was designed by combining the process variables and feedstock variables. Experiments were carried out at four different stagnation temperatures and at three different stagnation pressures for different powder feed rates for each powder. The parameters chosen for each variable were based on the equipment capability and the nature of the powder being sprayed so as to include the entire possible range. Five different powders were used: copper fine (Innomet), copper coarse (Innomet), alumina (105SPF, Metco), WC-12Co fine (Amperit 515, HC Stark) and WC-12Co coarse (71NS, Metco). In all, 72 experiments were carried out and each experiment was repeated 3 times for better statistics and repeatability studies.

Table 1 Experimental matrix

Exp No	Temperature, K	Pressure, MPa	Feed rate, g/min	Mean size, μm
A. Copper powder, D_p = 33 μm, ρ_p = 8910 kg/m^3				
A1	303	1	11	
A2	303	1.5	11	
A3	303	2	11	
A4	303	1	18	
A5	303	1.5	18	
A6	303	2	18	
A7	303	1	29	
A8	303	1.5	29	
A9	303	2	29	
A10	473	1	18	
A11	473	1.5	18	
A12	473	2	18	
A13	573	1	18	
A14	573	1.5	18	
A15	573	2	18	
A16	723	1	11	
A17	723	1.5	11	
A18	723	2	11	
A19	723	1	18	
A20	723	1.5	18	
A21	723	2	18	
A22	723	1	29	
A23	723	1.5	29	
A24	723	2	29	
B. Copper powder, D_p = 104 μm, ρ_p = 8910 kg/m^3				
B1	303	1	11	
B2	303	1.5	11	
B3	303	2	11	
B4	303	1	18	
B5	303	1.5	18	
B6	303	2	18	
B7	303	1	29	
B8	303	1.5	29	
B9	303	2	29	
B10	473	1	18	
B11	473	1.5	18	
B12	473	2	18	
B13	573	1	18	
B14	573	1.5	18	
B15	573	2	18	
B16	723	1	11	
B17	723	1.5	11	
B18	723	2	11	
B19	723	1	18	
B20	723	1.5	18	
B21	723	2	18	
B22	723	1	29	
B23	723	1.5	29	
B24	723	2	29	
C. Alumina powder, D_p = 35 μm, ρ_p = 3900 kg/m^3				
C1	303	1	11	
C2	303	1.5	11	
C3	303	2	11	
C4	303	1	18	
C5	303	1.5	18	
C6	303	2	18	
C7	303	1	29	
C8	303	1.5	29	
C9	303	2	29	
C10	473	1	18	
C11	473	1.5	18	
C12	473	2	18	
C13	573	1	18	
C14	573	1.5	18	
C15	573	2	18	
C16	723	1	18	
C17	723	1.5	18	
C18	723	2	18	
D. Wc-Co powder, ρ_p = 14500 kg/m^3				
D1	303	2	18	22
D2	523	2	18	22
D3	773	2	18	22
D4	303	2	18	56
D5	523	2	18	56
D6	773	2	18	56

Powder morphology was observed using a scanning electron microscope (Hitachi—S3400N, Japan). Table 1 provides the details of the process as well as the feedstock parameters used for each experiment along with the experiment numbers.

2.2 Particle Velocity Measurement

The powder particles were imaged using a high-speed imaging system (SprayWatch 2i, Oseir Ltd., Finland). A diode laser-based system (HiWatch) was used for illuminating the particles. It is essentially a time-of-flight technique in which the laser unit emits three pulses for a given camera exposure time. The pulse frequency and duration is adjusted based on the velocity range being measured. The distance travelled by the particle between the pluses estimated based on image processing, is then used to calculate the particle velocity. The particle size is estimated from the images of the particles based on the pixel count. Unlike the earlier studies, the present experimental setup involves background illumination as against a sheet laser as shown in Fig. 1. The present setup thus captures the particle shadow and is more effective than the sheet laser-based system due to greater depth of the field of view. Also, in the sheet laser-based system alignment of the laser sheet and the particle flow plane is very critical for reliable measurements, which is not the case with the present technique. The data presented for each experiment in the present study is averaged over thousands of particles.

3. Results and Discussion

3.1 Powder Characterization

The morphologies of the different powders used in the present study are shown in Fig. 2. The copper powders (fine and coarse) and tungsten carbide cobalt powder (fine) have near spherical morphologies, while, the alumina powder is found to be angular. The particle size distribution measured using the SprayWatch/HiWatch optical diagnostic system is shown in Fig. 3. The values of D10 (which denotes the diameter value below which 10%

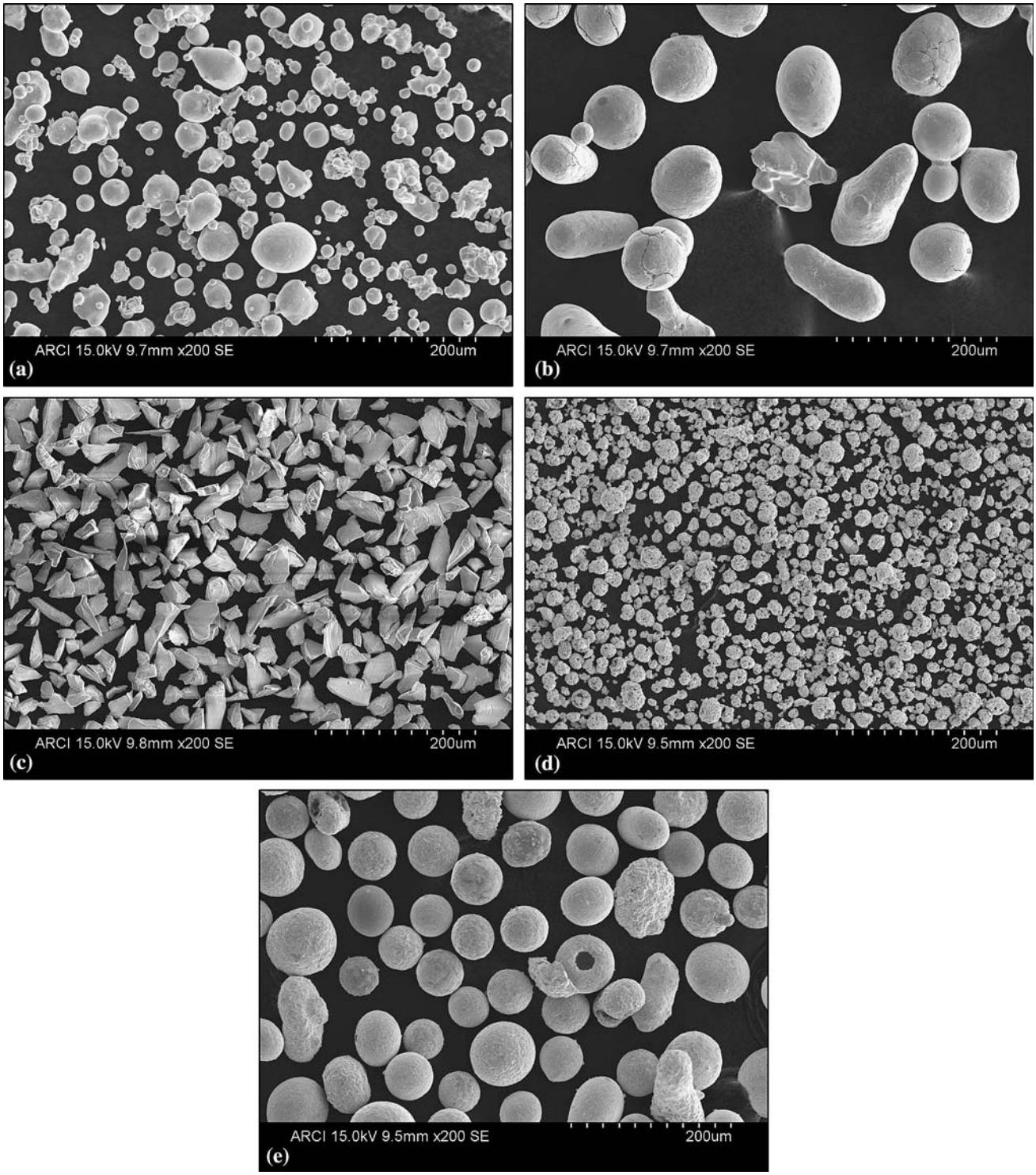

Fig. 2 SEM micrographs of (a) fine Copper (b) coarse Copper (c) fine Alumina (d) fine WC-12Co, and (e) coarse WC-12Co

of particles lie) and D90 (diameter value below which 90% of particles lie), along with the mean size, are also provided in the plots. Particle size was also estimated using Malvern Laser technique. In this technique, the powder particles are dispersed in a liquid medium on which a laser beam is incident and the particle size is determined based on an analysis of the diffracted laser beam. The difference in the sizes calculated by this technique and the SprayWatch diagnostic system was consistently found to be less than 10%. This difference is

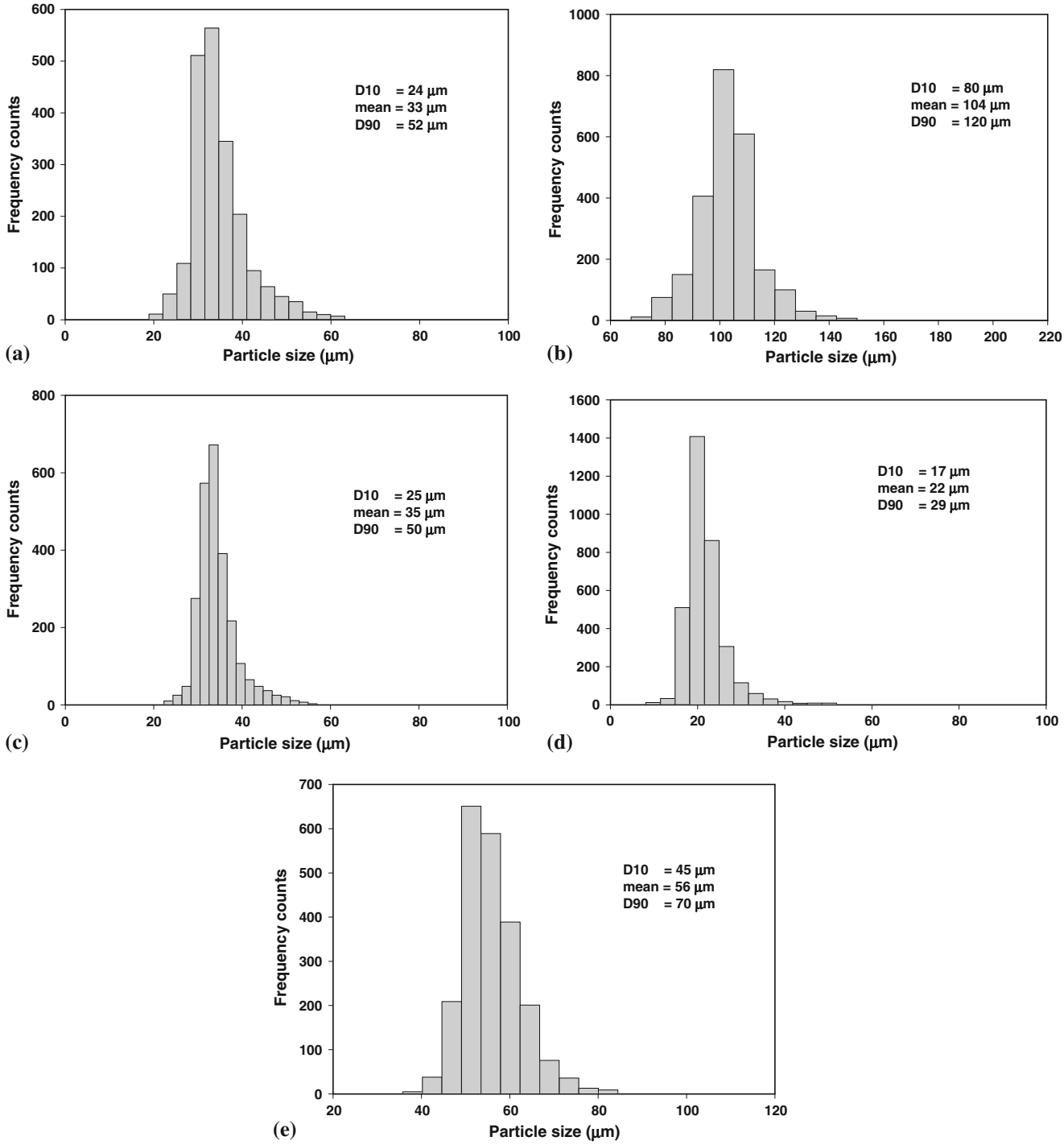

Fig. 3 The particle size distribution measured using the optical diagnostic system for (a) fine Copper (b) coarse Copper (c) fine Alumina (d) fine WC-12Co, and (e) coarse WC-12Co

possibly due to the lower accuracy levels of the diagnostic system and also the experimental errors associated with the manual focusing during the measurements. However, it is clear that the optical diagnostics data is consistent with the data from the laser-based measurement. All the powders used have a reasonably narrow size distribution, which is ideal for modeling studies.

3.2 Particle Velocity Profiles

The typical particle velocity profiles at the exit of the nozzle for the different powders are shown in Fig. 4. The profiles are straight lines normal to the flow direction. The velocity profiles remain constant almost upto the nozzle edges which clearly shows the advantage of the rectangular exit in comparison to the circular exit which results in a

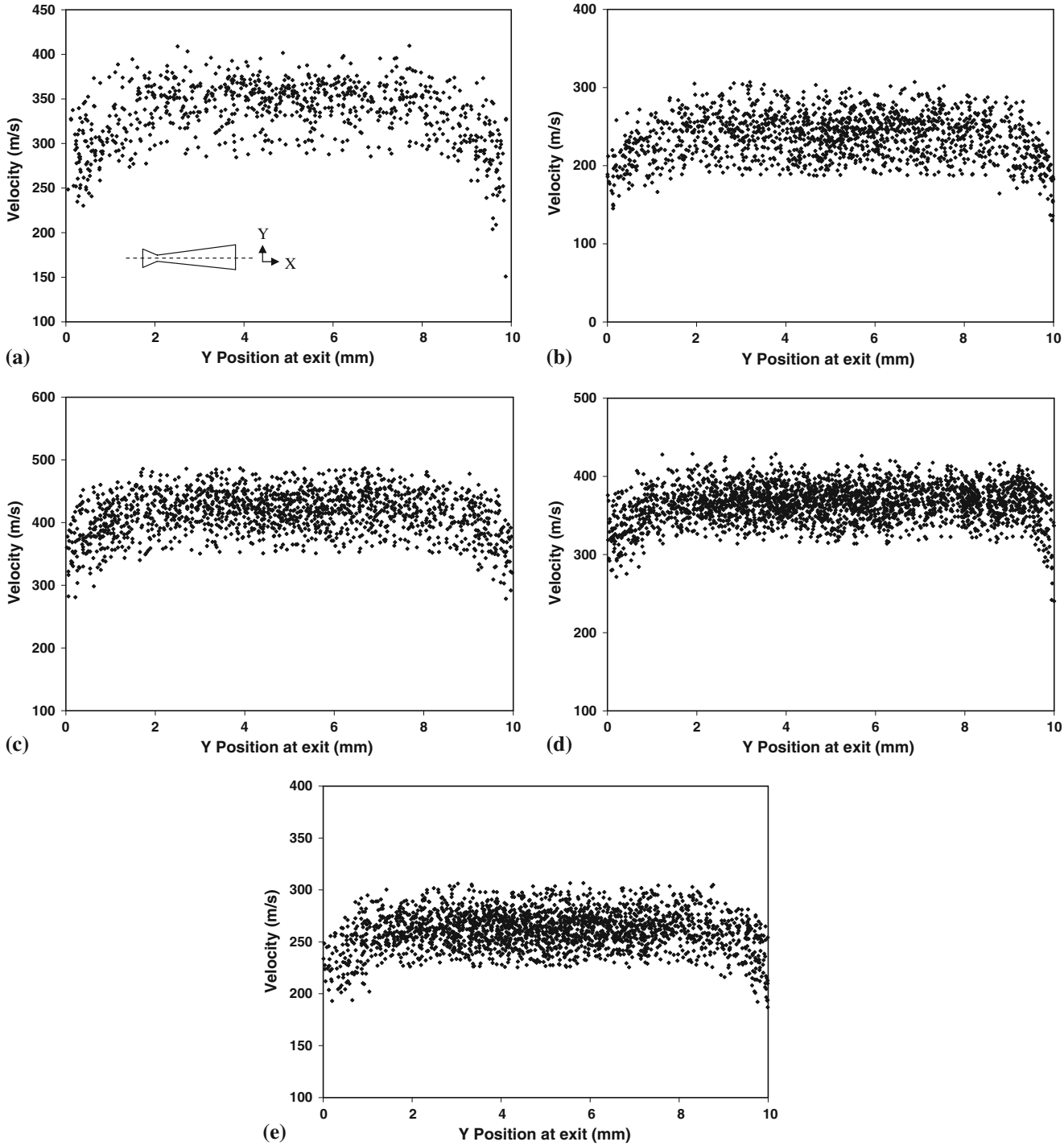

Fig. 4 Typical particle velocity profiles at the exit of the nozzle along the Y direction for (a) fine Copper (b) coarse Copper (c) fine Alumina (d) fine WC-12Co, and (e) coarse WC-12Co

parabolic velocity profile (Ref 14) with considerable difference between mean velocity and centerline velocity (peak velocity). In all cases, over 90% of the nozzle width (except for 5% on each side) exhibited a constant velocity unlike the case of a circular nozzle. The scatter of the particle velocity from the mean is ±40-50 m/s and is mostly due to the scatter in the particle size.

3.3 Effect of Stagnation Temperature and Pressure

The variation of particle velocity as a function of stagnation temperature at different pressures for different powders is shown in Fig. 5. Particle velocities in the range 220-600 m/s was observed depending on the particle size,

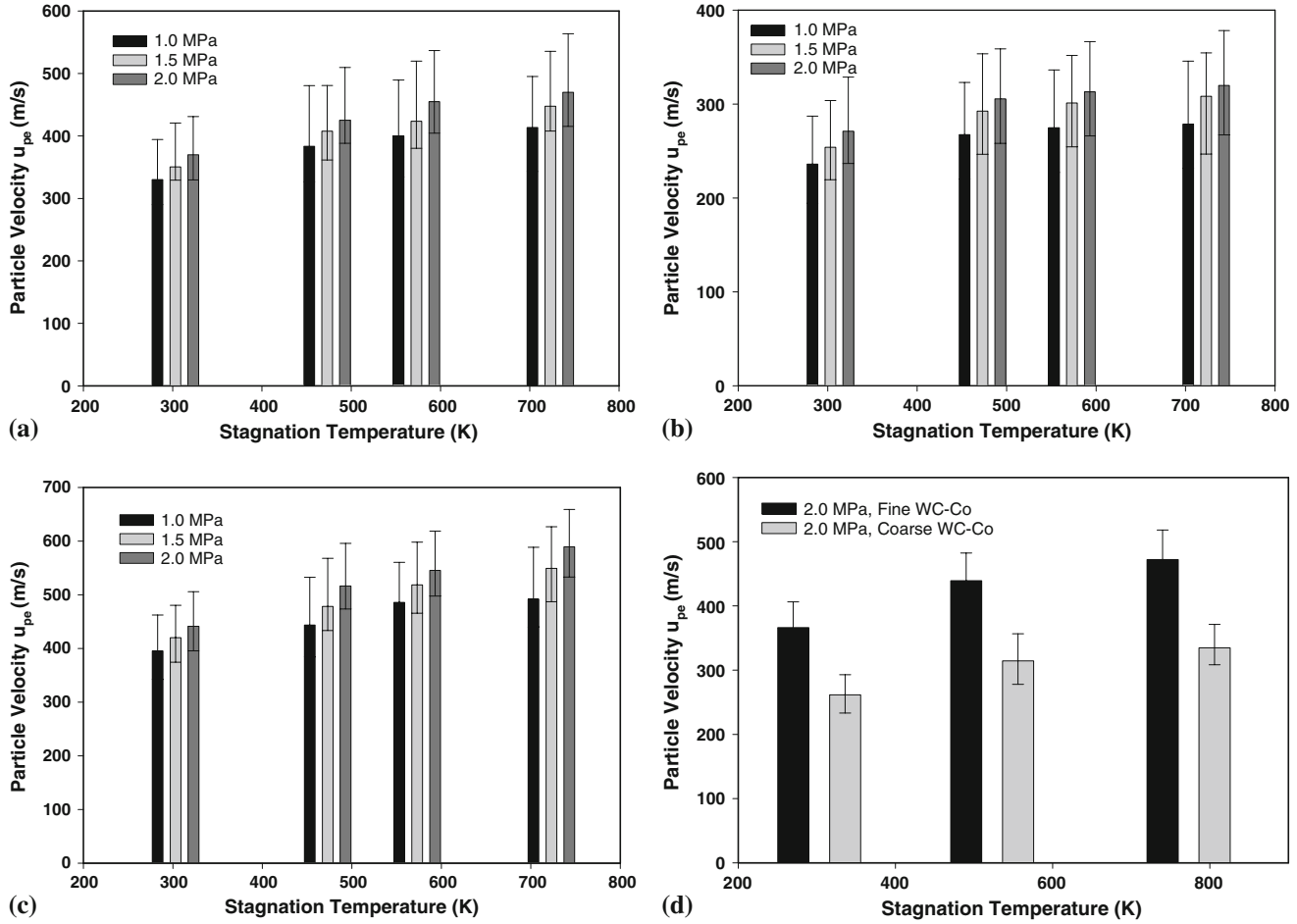

Fig. 5 Variation of particle velocity as a function of stagnation temperature for (a) fine Copper (b) coarse Copper (c) fine Alumina (d) fine WC-12Co and coarse WC-12Co

density, stagnation temperature and pressure. For all the powder particles, increasing stagnation temperatures increases the particle velocity. Similarly, increasing stagnation pressure (at a given stagnation temperature) also increases the particle velocity. Also, the trend is similar (non linear) at all the stagnation pressures. This indicates the absence of interdependence between stagnation temperature and other parameters (stagnation pressure, particle size, and particle density) in the resulting particle velocity. The plot also shows the considerable influence of stagnation pressure. Unlike the case of stagnation temperature, particle velocity scales linearly with stagnation pressure. The trend is again almost identical for all the powders as also observed in the case of stagnation temperature. This indicates the absence of interdependence between stagnation pressure and other parameters (stagnation temperature, particle size and particle density) in the resulting particle velocity. Hence it may be inferred that stagnation temperature and stagnation pressure have similar effect on particle velocity.

3.4 Effect of Powder Feed Rate

The variation of particle velocity as a function of powder feed rate for copper powder is shown in Fig. 6. The plot clearly shows the lack of any significant effect of feed rate on particle velocity in the present case, as also reported in earlier studies (Ref 12). Similar trend was observed for the other powders as well and a maximum change of around 9% in the particle velocity is observed for the different powder feed rates. The plots clearly indicate the absence of particle loading effect on particle velocity for the range explored in the present study. This is possibly due to the very low concentration of the particles in the gas ($<1\%$ by mass). This observation also strengthens the assumption of absence of particle loading effect on the gas flow conditions, being employed in the particle acceleration model in the later sections of this article. Hence, particle feed rate has not been considered for subsequent analysis.

3.5 Effect of Particle Mass

The variation of particle velocity as a function of particle mass at a stagnation pressure of 2.0 MPa and stagnation temperature of 303 K (room temperature) is shown in Fig. 7. From the plot it may be inferred that particle mass has significant effect on particle velocity. The plot also clearly indicates the inability to accelerate heavier

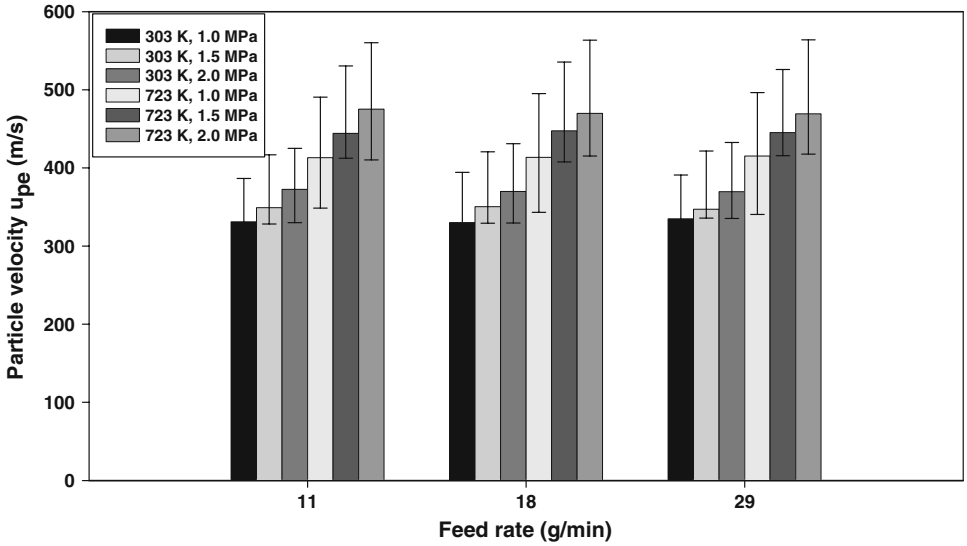

Fig. 6 Variation of particle velocity as a function of powder feed rate for fine Copper

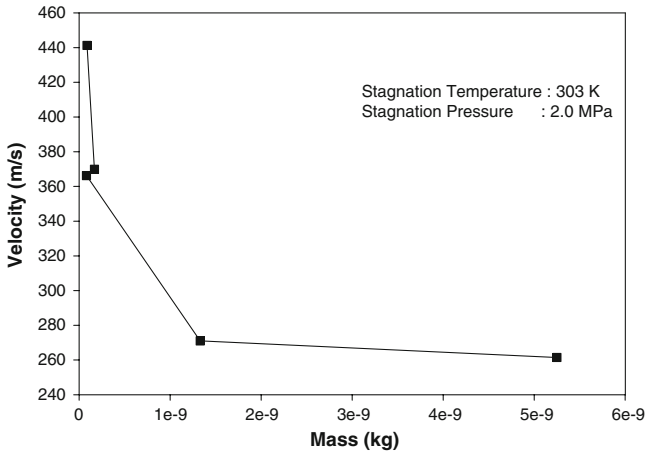

Fig. 7 Variation of particle velocity as a function of particle mass

powder particles (coarse copper and tungsten carbide) at the process parameters employed. This aspect is discussed in greater detail in the subsequent sections.

3.6 Relative Influence of Process and Feedstock Parameters

To determine the influence of process and feedstock parameters, multiple linear regression analysis was carried out with stagnation temperature, stagnation pressure, powder feed rate, particle size, and density as independent variables and the particle velocity as the dependent variable using the following scheme.

$$\overline{u}_{\mathrm{p}} = m_1\overline{T} + m_2\overline{P} + m_3\overline{FR} + m_4\overline{D}_{\mathrm{p}} + m_5\overline{\rho}_{\mathrm{p}} + \mathrm{K} \qquad \text{(Eq 1)}$$

where, m_1 to m_5 are the corresponding regression coefficients and K is the constant. The data for each of the independent variable was normalized to enable direct comparison of the regression coefficient for each of the independent variable to ultimately calculate the relative influence of process parameters as well as the feedstock parameters. Normalization was carried out using the equation shown below.

$$\overline{a}_{i,j} = 0.1 + \left(\frac{a_{i,j} - a_{j\min}}{a_{j\max} - a_{ji\min}}\right)0.8 \qquad \text{(Eq 2)}$$

for $i = 1\text{-}72$ (total number of experiments and $j = 1\text{-}5$) (stagnation temperature, stagnation pressure, powder feed rate, particle size, and density, respectively)

where, a is the matrix containing the data of the independent variables and $\overline{a}$ is the normalized matrix of the same being used for regression analysis.

The regression coefficients for the process, as well as the feedstock parameters determined by the multiple linear regression analysis, are plotted in Fig. 8. The regression coefficients indicate the relative influence of the parameters. Higher the absolute value of the coefficient, greater is its influence. The sign of the coefficient also indicates if the parameter influences the particle velocity positively or negatively. Increasing the stagnation temperature and pressure is found to have positive effect on particle velocity while increasing powder particle size and density has retarding effect. The plot clearly shows the dominant effect of the feedstock parameters as also observed in the results presented in the earlier sections. The coefficients for particle size and density are almost identical indicating the importance of particle mass as also evident from Fig. 7. Also, among the process parameters stagnation temperature has the most dominant effect as also experimentally observed in an earlier work of the authors (Ref 20). The lack of any significant influence of powder feed rate is also clearly reinforced by the present regression analysis.

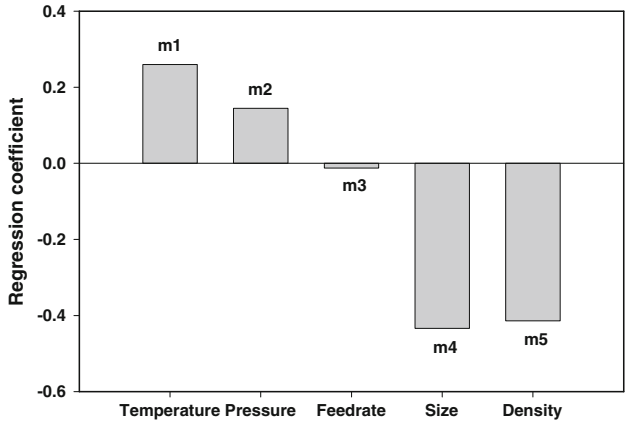

Fig. 8 Variation of regression coefficient for process and feed stock parameters

4. Mathematical Model for Particle Velocity

In this section, a mathematical model is being presented to determine the particle velocity for different gas inlet conditions and feedstock parameters for the flow through a De Laval nozzle shown in Fig. 9. Initially a gas dynamic model is employed to determine the gas flow conditions and then a particle acceleration model is used to determine the particle velocity for the flow field determined by the gas dynamic model.

4.1 Isentropic Gas Dynamic Model

An isentropic gas flow model is employed to determine the velocity, temperature and density of the gas at various locations in the nozzle. A De Laval nozzle with rectangular exit is used in the present study. The schematic of the nozzle is shown in Fig. 9. Inline with the approach adopted by Dykhuizen et al. (Ref 3) the model involves calculation of the velocity of sound in the medium (air in the present case) as a function of temperature, followed by calculation of properties of the gas as a function of local Mach number using the isentropic flow relationships and finally calculation of Mach number based on the nozzle geometry.

4.2 Particle Acceleration Model

Once the gas properties are determined using the gas flow model, the particle velocity is calculated using the drag force (F_D) on the particle (Ref 3) employing the following equation:

$$F_D = m\frac{du_p}{dt} = \frac{C_D \rho (u - u_p)^2 A_p}{2} \quad \text{(Eq 3)}$$

Assuming the particles to be spherical the above equation takes the form.

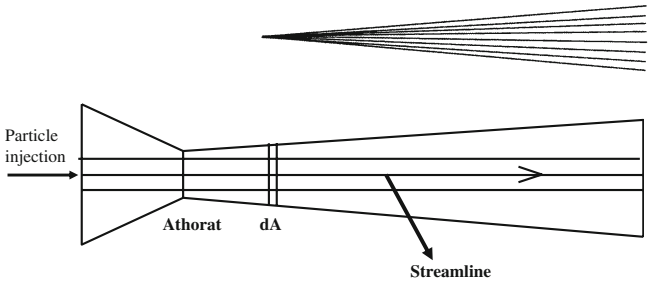

Fig. 9 Schematic of De Laval nozzle with rectangular exit

$$\frac{du_p}{dt} = \frac{3}{4} C_D \left(\frac{\rho}{\rho_p D_p}\right)(u - u_p)^2 \quad \text{(Eq 4)}$$

where, m is the mass of the particle, C_D is the drag coefficient, ρ is the gas density, u is the gas velocity, u_p is the particle velocity, A_p is the cross sectional area of the particle, ρ_p is the particle density, and D_p is the particle diameter.

The drag coefficient is calculated based on the model proposed by Henderson (Ref 21). Under the assumption that the particle loading is small enough not to affect the gas flow, the particle velocity can be determined by sequentially solving the gas flow model and the particle acceleration model.

4.3 Numerical Implementation

Stagnation pressure (P_o), stagnation temperature (T_o), nozzle geometry are user specified inputs. T_o was varied from 300 K to 773 K and P_o was varied from 1.0 MPa to 2.0 MPa while the diverging section length was 102 mm. The process gas was air having a γ (specific heat ratio) of 1.4 and a density of 1.27 kg/m^3 at conditions of standard temperature and pressure, STP (273.15 K and 0.101325 MPa). With these inputs the flow conditions at the throat can be calculated using the gas flow model. The flow conditions at various locations in the nozzle are calculated by using the flow conditions at the throat and the corresponding local flow area and local Mach number. At the end of each time step the particle velocity is computed. The solution could be marching in 'time' or 'displacement'. The accuracy of the solution depends on the time step chosen, which is typical of any marching solution. The time step was appropriately chosen to ensure good accuracy of the results.

4.4 Alkhimov's Empirical Model

Alkhimov et al. (Ref 4) proposed an empirical relationship to predict the particle velocity at the exit of the nozzle as a function of gas inlet conditions, feedstock conditions and nozzle geometry as shown below.

$$u_{pe} = \frac{u_e}{1 + 0.85\sqrt{\frac{D_p}{X_d}}\sqrt{\frac{\rho_p u_e^2}{P}}} \quad \text{(Eq 5)}$$

where, u_{pe} is the particle velocity at the exit of the nozzle, u_e is the gas velocity at the exit of the nozzle, P is the gas inlet pressure, and X_d is the length of the diverging section of the nozzle.

The above empirical equation is used to calculate the particle velocity for all the experimental conditions specified in Table 1 and the results are compared with the experimental data in the subsequent section.

5. Comparison of Modeling and Experimental Results

In this section initially, some insights into nozzle design for different feedstock parameters are provided and subsequently the model predictions are compared with the experimental results and also other models in the literature.

5.1 Influence of Nozzle Length

To assess the effect of length of diverging section of the nozzle on particle velocity for powders of different sizes and densities the variation of ratio of particle velocity to gas velocity (u_p/u) from the throat to the exit of the nozzle for an inlet gas temperature and pressure of 303 K and 2.0 MPa, respectively, is plotted in Fig. 10a. The symbol X in the figure gives the distance in the diverging section along the axis of the nozzle, measured from the throat. The plot shows the greater acceleration levels in fine and low density alumina powder with u_p/u in excess of 0.7 at X_D = 102 mm whereas, coarse and dense copper and tungsten carbide cobalt powders have a value of around 0.4 at X_D = 102 mm. This indicates that there is greater scope for acceleration in these powders. To gain more insights into the driving force for particle acceleration in the diverging section, (u-u_p) is plotted as a function of distance from throat in Fig. 10b. The plot clearly brings out the difference in the acceleration levels (u-u_p) for the different powders. The coarse copper and tungsten carbide powders have an almost constant difference in particle and gas velocities unlike the other powders, which can be attributed to the higher mass of these particles. To look into possible ways of achieving greater velocities, the effect of all the parameters on particle velocity is summarized in Fig. 11. In this plot, variation of particle velocity with stagnation temperature, stagnation pressure, particle density, size and length of diverging section of the nozzle is presented. Each parameter is varied at a time while maintaining the base values for all the others parameters. The base values are specified in the plot. The alphabets T, P, L, and S shown on the X-axis stand for the stagnation temperature, stagnation pressure, length of diverging section and particle size while the numbers shown after the alphabets are the values of the respective parameters. Stagnation temperature, stagnation pressure and length of diverging section have positive influence on particle velocity while density and size have retarding effect. Hence, it may be inferred form the plot that for higher density powders a combination of higher temperatures and pressures are required. Also it is preferable to use a finer particle size and longer nozzle for these cases. It is worth noting that as the present model does not consider the effect of deceleration of the gas due to the particle loading, it predicts an increase in particle velocity even for very long diverging section length. However, Fig. 11 could provide guidelines for appropriate selection of process parameters based on the powder to be

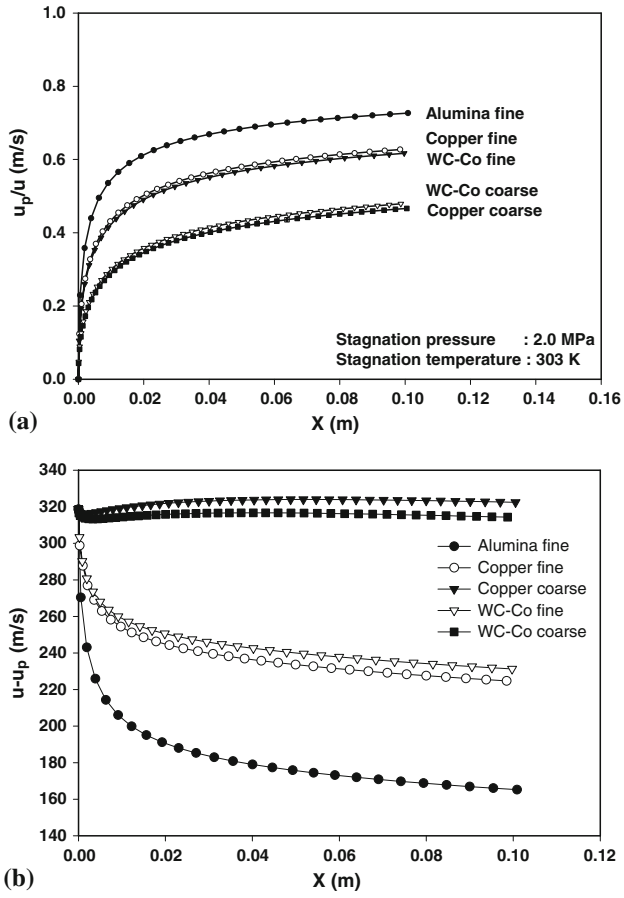

Fig. 10 Variation of (a) u_p/u (b) u-u_p with distance from the throat

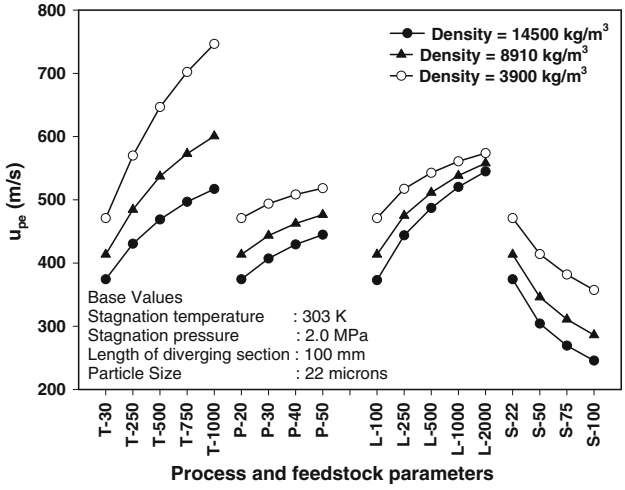

Fig. 11 Variation of particle velocity for different process parameters

deposited and the capability of the coating system being employed.

5.2 Prediction of Particle Velocity

The particle velocity predicted by the model presented in the earlier section is compared with the experimental results for copper powder at different parameters in Fig. 12a. The numbers adjacent to the points denote the experiment number as detailed in Table 1. The plot clearly shows the excellent predictability of the model over a wide range of gas inlet conditions. Similar results were observed for all the powders and the results for all the experiments are consolidated in Fig. 12b. The plots clearly indicate the good prediction capability of the model over a wide range of process parameters and feedstock conditions. Hence, the present model stands validated and the assumptions made in the model formulation may be considered to be very reasonable. The predictions of Alkhimov model are compared with the experimental results in Fig. 12c. Even in this case excellent predictability is observed indicating the possible use of the empirical equation for velocity calculations given the ease of calculation.

5.3 Scatter in Particle Velocity

In order to understand the experimentally observed scatter in particle velocity at the nozzle exit (see Fig. 4), the measured scatter in particle velocity (Δu_p—velocity band shown in Fig. 4) was compared to the velocity scatter calculated based on the scatter in particle size (size range given by D10 and D90) and $\Delta u_p/u_{p(avg)}$ was plotted for experimental and predicted data as shown in Fig. 13a. The data for all the experiments is found to lie within a narrow band. From the plot it is clear that the experimentally observed scatter in the particle velocity is largely due to the powder particle size distribution. To clearly understand the effect of particle size dispersion, the velocity dispersion ($\Delta u_p/u_{p(avg)}$) was plotted against size dispersion ($\Delta D_p/D_p$) for the different powders and particle sizes in Fig. 13b and c. From the plots it may be inferred that, for a given density (ρ_p) and mean particle size (D_p), the velocity dispersion ($\Delta u_p/u_{p(avg)}$) almost linearly scales with size dispersion ($\Delta D_p/D_p$). For a given size dispersion ($\Delta D_p/D_p$), the velocity dispersion is more at higher mean particle sizes (D_p) and distribution (ΔD_p). Also, for a given size dispersion ($\Delta D_p/D_p$), the velocity dispersion is more for denser particles. From this it is clear that the velocity dispersion does indeed scale almost linearly with the size dispersion for a given powder density and mean particle size, indicating the need to use powders with narrow size distribution.

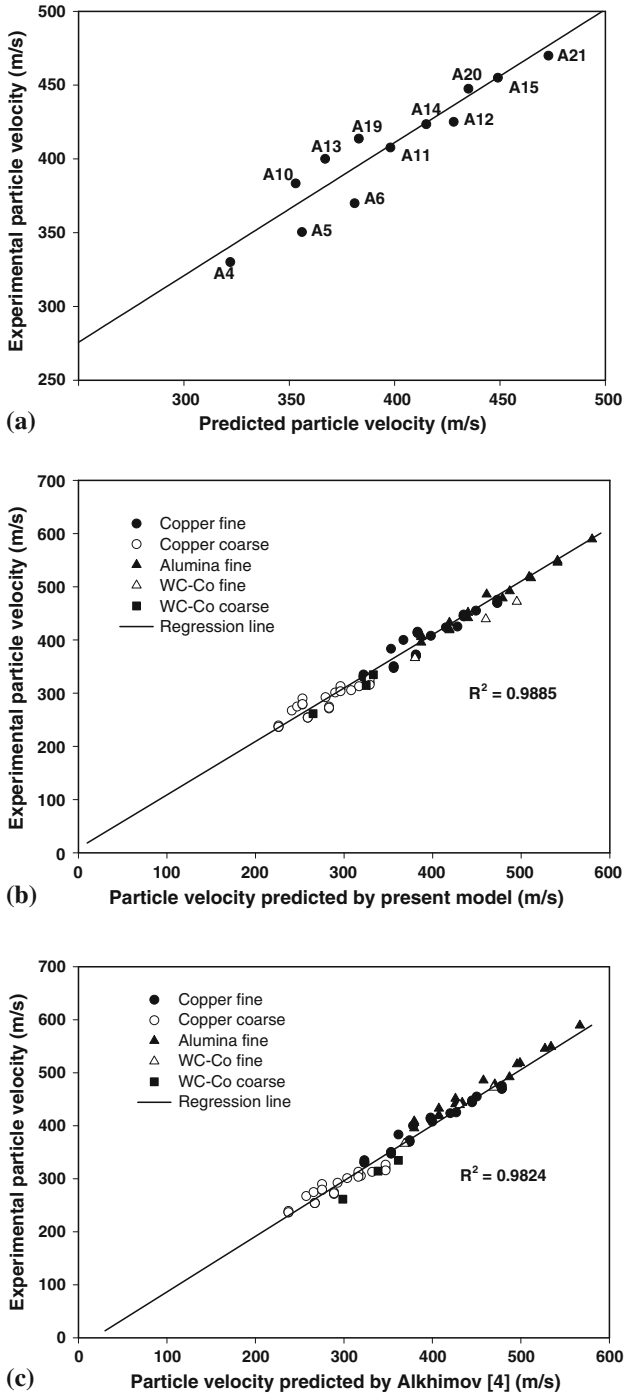

Fig. 12 Comparison of modeling and experimental particle velocities (a) present model for fine copper (b) present model for all powders (c) Alkhimov model

6. Conclusions

- High-speed camera with laser illumination-based particle diagnostic system has been successfully able to capture the velocity profiles for a De Laval nozzle with rectangular exit over a wide range of stagnation temperature, stagnation pressure, particle size and particle density and the results compare well with the model predictions.
- Stagnation temperature is found to have greater influence on particle velocity in comparison to stagnation pressure.

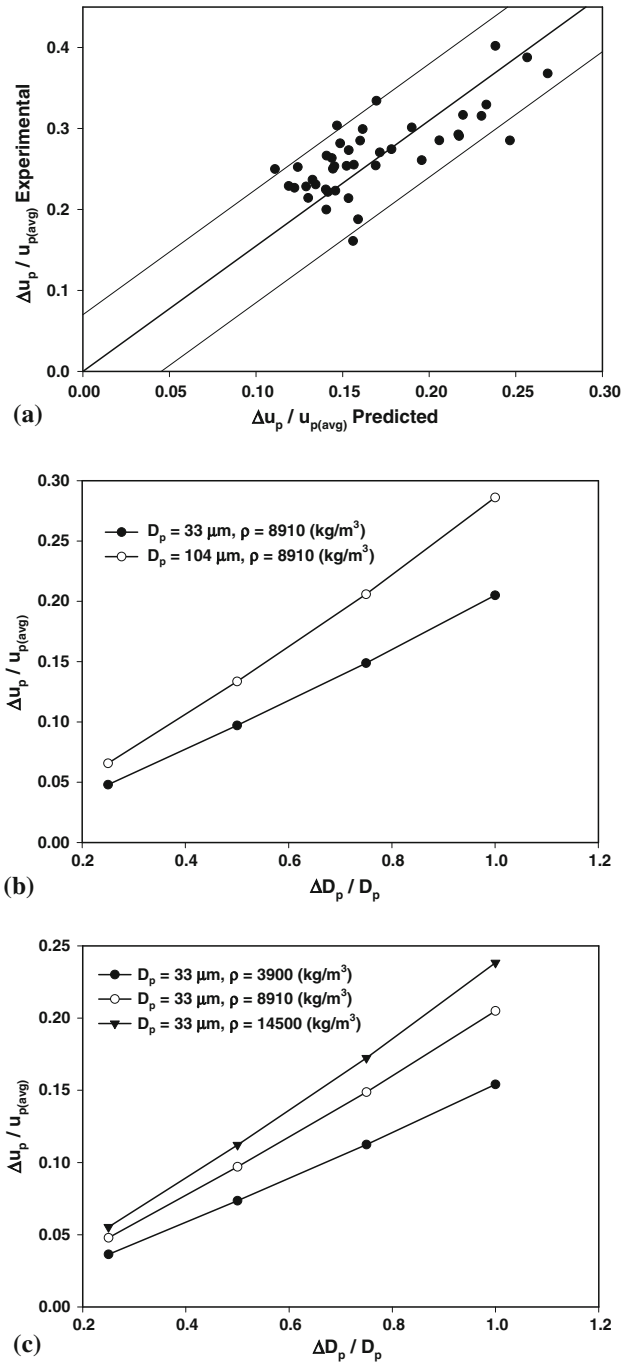

Fig. 13 Variation of (a) experimental and predicted scatter in particle velocity (b) velocity dispersion with size dispersion at different particle sizes (c) velocity dispersion with size dispersion for different powder densities

- Powder feed rate (particle loading) is found to have negligible effect on particle velocity for the range employed in the present study due to the lower particle concentrations in the present study.
- Feedstock parameters (particle size and particle density) are found to have greater influence on particle velocity compared to stagnation temperature and stagnation pressure.
- Interdependence between the process parameters and feedstock parameters in determining the particle velocity is found to be absent.
- The present study involving mathematical modeling along with experimental validation has provided a comprehensive picture of the effect of process parameters and the feedstock parameters on the particle velocity for a De Laval nozzle with rectangular exit used for cold spraying, which could be of great help in not only understanding the underlying science, but also to tailor the process to meet the market requirements.

References

1. A.P. Alkhimov, A.N. Papyrin, V.F. Kosarev, N.J. Nesterovich, and M.M Shuspanov, ''Gas Dynamic Spraying Method for Applying a Coating,'' U.S. Patent 5,302,414, April 12, 1994
2. R.C. Dykhuizen, M.F. Smith, D.L. Gilmore, R.A. Neiser, X. Jiang, and S. Sampath, Impact of High Velocity Cold Spray Particles, *J. Thermal Spray Technol.*, 1999, **8**(4), p 559-564
3. R.C. Dykhuizen and M.F. Smith, Gas Dynamic Principles of Cold Spray, *J. Thermal Spray Technol.*, 1998, **7**(2), p 205-212
4. A.P. Alkhimov, V.F. Kosarev, and S.V. Klinkov, The Features of Cold Spray Nozzle Design, *J. Thermal Spray Technol.*, 2001, **10**(2), p 375-381
5. B. Jodoin, Cold Spray Nozzle Mach Number Limitation, *J. Thermal Spray Technol.*, 2002, **11**(4), p 496-507
6. T. Stoltenhoff, H Kreye, and H.J. Richter, An Analysis of the Cold Spray Process and Its Coatings, *J. Thermal Spray Technol.*, 2002, **11**(4), p 542-550
7. M. Grujicic, C.L. Zhao, C. Tong, W.S. DeRosset, and D. Helfritch, Analysis of the Impact Velocity of Powder Particles in the Cold-Gas Dynamic-Spray Process, *Mater Sci. Eng. A*, 2004, **368**, p 222-230
8. W.-Y. Li, H. Liao, G. Douchy, and C. Coddet, Optimal Design of Cold Spray Nozzle by Numerical Analysis of Particle Velocity and Experimental Validation with 316L Stainless Steel Powder, *Mater. Design*, 2007, **28**, p 2129-2137
9. W.-Y. Li, H. Liao, H.-T. Wang, C.-J. Li, G. Zhang, and C. Coddet, Optimal Design of Convergent-Barrel Cold Spray Nozzle by Numerical Method, *Appl. Surf. Sci.*, 2006, **253**, p 708-713
10. T.-C. Jen, L. Li, W. Cui, Q. Chen, and X. Zhang, Numerical Investigations on Cold Gas Dynamic Spray Process with Nano and Micro Size Particles, *Int. J. Heat Mass Trans.*, 2005, **48**, p 4384-4396
11. T. Marrocco, D.G. McCartney, P.H. Shipway, and A.J. Sturgeon, Production of Titanium Deposits by Cold-Gas Dynamic Spray: Numerical Modeling and Experimental Characterization, *J. Thermal Spray Technol.*, 2006, **15**(2), p 263-272
12. K. Taylor, B. Jodoin, and J. Karov, Particle Loading Effect in Cold Spray, *J. Thermal Spray Technol.*, 2006, **15**(2), p 273-279
13. B. Jodoin, F. Raletz, and M. Vardelle, Cold Spray Modeling and Validation Using an Optical Diagnostic Method, *Surf. Coat. Technol.*, 2006, **200**, p 4424-4432
14. J. Wu, H. Fang, S. Yoon, H. Kim, and C. Lee, Measurement of Particle Velocity and Characterization of Deposition in Aluminum Alloy Kinetic Spraying Process, *Appl. Surf. Sci.*, 2005, **252**, p 1368-1377
15. H. Fukanuma, N. Ohno, B. Sun, and R. Huang, In-flight Particle Velocity Measurements with DPV-2000 in Cold Spray, *Surf. Coat. Technol.*, 2006, **201**, p 1935-1941
16. X.-J. Ning, J.-H. Jang, and H.-J. Kim, The Effect of Powder Properties on In-flight Particle Velocity and Deposition Process During Low Pressure Cold Spray Process, *Appl. Surf. Sci.*, 2007, **253** , p 7449-7455

17. M. Karimi, A. Fartaj, G. Rankin, D. Vnaderzwet, W. Birtch, and J. Villafuerte, Numerical Simulation of the Cold Gas Dynamic Spray Process, *J. Thermal Spray Technol.*, 2006, **15**(4), p 518-523
18. W.-Y. Li, C.-J. Li, H.-T. Wang, C.-X. Li, and H.-S. Bang, Measurement and Numerical Simulation of Particle Velocity in Cold Spraying, *J. Thermal Spray Technol.*, 2006, **15**(4), p 559-562
19. J. Karthikeyan, C.M. Kay, J. Lindeman, R.S. Lima, and C.C. Berndt, Cold Spray Processing of Titanium Powder, *Thermal Spray: Surface Engineering via Applied Research*, C.C. Berndt, Ed., May 8-11, 2000 (Montreal, Quebec, Canada), ASM International, 2000, p 255-262
20. P. Sudharshan Phani, D. Srinivasa Rao, S.V. Joshi, and G. Sundararajan, Effect of Process Parameters and Heat Treatments on Properties of Cold Sprayed Copper Coatings, *J. Thermal Spray Technol.*, 2007, **16**, p 425-434
21. C.B. Henderson, Drag Coefficients of Spheres in Continuum and Rarefied Flows, *AIAA J.*, 1976, **14**(6), p 707-708